Photocatalysis
https://www.sciltp.com/journals/photocatalysis

Article

Check for updates

Coupled Light-Driven *p*-Xylene Oxidation and H_2O_2 Production with Organic Photocatalysts in Propylene Carbonate

Tao Wu [1,†], Arianna Gentilin [1,†], Federico Droghetti [2], Luca Morhart [1,3], Luka Đorđević [1,*], Mirco Natali [2,*] and Andrea Sartorel [1,*]

[1] Department of Chemical Sciences (DiSC), University of Padova, 35131 Padova, Italy
[2] Department of Chemical, Pharmaceutical and Agricultural Sciences (DOCPAS), University of Ferrara, 44121 Ferrara, Italy
[3] Institute of Organic Chemistry, Justus Liebig University Giessen, 35390 Giessen, Germany
* Correspondence: luka.dordevic@unipd.it (L.Đ.); mirco.natali@unife.it (M.N.); andrea.sartorel@unipd.it (A.S.)
† These authors contributed equally to this work.

How To Cite: Wu, T.; Gentilin, A.; Droghetti, F.; et al. Coupled Light-Driven *p*-Xylene Oxidation and H_2O_2 Production with Organic Photocatalysts in Propylene Carbonate. *Photocatalysis* **2026**, *2*(3), 7. https://doi.org/10.53941/photocatalysis.2026.100007

Received: 15 June 2026
Revised: 13 July 2026
Accepted: 24 July 2026
Published: 4 August 2026

Abstract: The aerobic photocatalytic oxidation of *p*-xylene to *p*-tolualdehyde (*p*-TALD) is reported here in propylene carbonate as a green solvent under visible light irradiation using organic photocatalysts, such as 9,10-anthraquinone (AQ) and 3,6-di-*tert*-butyl-9-mesityl-10-phenylacridinium (Acr^+-1). Optimized conditions achieved up to 80–84% *p*-xylene conversion in 24 h, with *p*-TALD as the main product (up to 44% yield, 60% selectivity). The photooxidation is coupled to dioxygen reduction for H_2O_2 production, reaching concentrations up to 27 mM. Mechanistic investigation by laser flash photolysis and electron paramagnetic resonance spectroscopy revealed a non-innocent role of propylene carbonate, which promotes reductive quenching of ^{3}*AQ, generating the radical anion $AQ^{\bullet-}$ and dianion AQ^{2-} reduced species of the photocatalyst. Upon aerobic oxidation, these are responsible for generation of reactive oxygen species such as superoxide radical anion ($O_2^{\bullet-}$) and hydrogen peroxide (H_2O_2). The oxidation of *p*-xylene proceeds through a radical chain mechanism initiated by hydrogen atom transfer. The photocatalytic conditions were extended to other substrates bearing activated C–H bonds, demonstrating broad synthetic applicability.

Keywords: organic photocatalyst; *p*-xylene; hydrogen peroxide; green solvent; reactive oxygen species

1. Introduction

Photocatalysis is one of the main pillars in several natural and artificial processes aimed at the production of solar fuels [1–3], at water/air remediation [4–6] or at developing sustainable organic transformations [7,8]. These latter include oxidative valorization of abundant and critical feedstocks, leading to the production of value-added products in a sustainable way. Recent examples deal with the photocatalytic upcycling of plastic [9–12], biomass conversion [7,13], and selective transformation of strategic raw materials to fine chemicals [14,15].

In the context of oxidative valorization processes, particular attention is placed on *p*-xylene; its transformation to *p*-terephthalic acid (TA) through the Amoco process is by far the highest capacity industrial oxidation process of organic compounds. Intermediate oxidation products such as *p*-methylbenzyl alcohol (*p*-MA), *p*-tolualdehyde (*p*-TALD) or *p*-toluic acid (*p*-TA) retain synthetic interest (Scheme 1). The oxidation of *p*-xylene typically proceeds through the functionalization of activated benzylic C−H bonds, characterized by a low bond dissociation free energy (BDFE) of around 80 kcal mol^{-1} and thus amenable through reactivity via hydrogen atom transfer (HAT) [16]. Moreover, in photocatalytic oxidation of *p*-xylene, the main product obtained often depends

on the specific conditions adopted and on the overall conversion of *p*-xylene, since reactive oxygen species (ROS) can pertain in the oxidative cycle.

Thus, photocatalytic oxidation of *p*-xylene has been previously considered with inorganic photocatalysts such as TiO_2 nanoparticles [17,18] and tetrabutylammonium decatungstate [19] (TBADT), which operate both in the UV region (365 nm, Scheme 1). Other studies involved the use of organic photocatalysts to expand the utilization of light towards the visible region; in particular anthraquinones with carboxylic group (AQ-COOH) [20] and 9-mesityl-2,7,10-trimethylacridinium (Acr^+-Mes) [21] were employed in acetone and in a mixture of $CH_3CN/H_2O/H_2SO_4$, respectively. More recently, an acetonitrile-based photocatalytic system using the tetraaza-macrocyclic iron complex FeBr(pyclen) was employed as a photocatalyst for *p*-xylene oxidation, through the generation of Br• radicals capable of HAT [22].

Current efforts have thus been dedicated to developing new photocatalysts, possibly exploiting the visible region of solar emission. However, the development of sustainable and scalable photocatalytic processes should also consider the general conditions adopted, in particularly avoiding hazardous solvents and additives.

In this work, we apply organic photocatalysts from the families of quinones and acridinium ions for the aerobic oxidation of *p*-xylene in propylene carbonate as a green solvent [23]. This enables the selective photooxidation of *p*-xylene to *p*-TALD as the main product, while concomitantly leading to the production of hydrogen peroxide (H_2O_2) [24] from O_2 reduction. Mechanistic investigation through laser flash photolysis (LFP) and electron paramagnetic resonance (EPR) spectroscopy highlight a non-innocent role of propylene carbonate, in activating a chain oxidation reaction. Further substrate scope supports a versatile utilization of the photocatalytic conditions, opening new future opportunities for sustainable oxidative transformations.

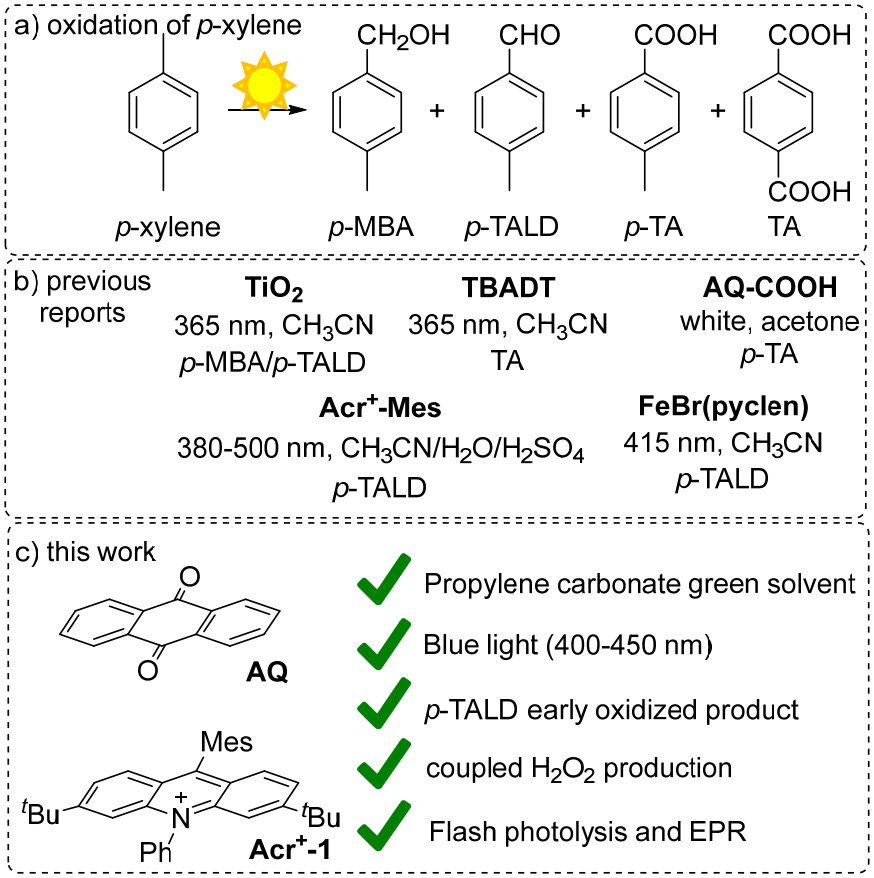

Scheme 1. (**a**) general scheme of *p*-xylene photooxidation with main reaction products represented; (**b**) previous reports; (**c**) presentation of this work.

2. Materials and Methods

Reagents and solvents including propylene carbonate, mesitylene, *p*-xylene, *o*-xylene, *m*-xylene, diphenylmethane, ethylbenzene, ethanol, anthraquinone, 3,6-di-tert-butyl-9-mesityl-phenylacridin-10-ium tetrafluoroborate, 3,3′,5,5′-tetramethylbenzidine (TMB) and horseradish peroxidase (HRP) were purchased from Merck and used as received. Photocatalysis experiments were conducted in 1 mL scale, in 8 mL glass vials under stirring (600 rpm), using homemade photoreactors with white or blue light (Figures S1 and S2), illuminating the vials from the bottom [7]. Progress of the

photocatalytic reactions was performed by ^{1}H-NMR (NMR=Nuclear Magnetic Resonance, Bruker Avance 400 III HD spectrometer, Bruker, Rheinstetten, Germany), using mesitylene as internal standard (6.80 ppm, singlet, 3H). δ for ^{1}H is given in ppm relative to the residual signal of the solvent (CD_3CN, quintet signal centered at 1.99 ppm). Multiplicities are indicated by *s* (singlet), *d* (doublet), *t* (triplet), *q* (quartet), *quint* (quintet), *m* (multiplet). The NMR spectra were processed using MestReNova software (Mestrelab Research, Santiago de Compostela, Spain). Identification of oxidation products was confirmed by gas chromatography coupled to mass spectrometry (GC-MS, Agilent Technologies, Santa Clara, CA, USA) analysis.

Quantification of H_2O_2 was performed through an optical method (Varian Cary 50 Scan UV-Visible spectrophotometer), via the oxidation of TMB by H_2O_2 catalyzed by HRP, leading to the formation of a blue charge-transfer complex (λ_{max} = 652 nm, $\varepsilon_{652} = 3.9 \times 10^4$ $M^{-1}cm^{-1}$) in 1:1 stoichiometry with respect to H_2O_2 [25,26].

Electron Paramagnetic Resonance spectra were acquired on a Bruker ESR5000 operating at a microwave frequency of 9.4 GHz. 25 μL of solution samples were introduced into capillaries and sealed. The AQ spectra were recorded using ESRStudio at room temperature with 1.0 mT microwave power, 0.02 mT modulation and 180 s sweep time. The AQ degassed sample was irradiated in situ using 405 nm LED (same used for photooxidation experiments) for 60 s. For the spin trap experiments, 5,5-dimethyl-1-pyrroline-*N*-oxide (25 mM DMPO, Merck code 92688) was introduced within the photocatalytic solution and irradiated for 30 s, before measuring the EPR signal (20 mW microwave power and 0.028 mT modulation, 60 s sweep time). The simulations were performed using the EasySpin software package (version 6.0.4) [27].

Laser flash photolysis measurements were conducted using a custom laser spectrometer comprising a Continuum Surelite II Nd: YAG laser (FWHM = 8 ns) with a frequency-tripled option (355 nm). Photomultiplier signals (kinetic traces) were processed by using a Teledyne LeCroy 604Zi (400 MHz, 20 GS/s) digital oscilloscope. Transient spectra were recorded using a PiMax CCD Camera.

Further details are reported in the Supplementary Materials.

3. Results

We started our investigation by screening several photocatalysts (PCs) in the aerobic light-driven oxidation of *p*-xylene (80 mM) in acetonitrile under air atmosphere and upon white light irradiation (33 mW cm^{-2}, i.e., 0.33 sun [7]). This investigation included quinoid derivatives, commercial aromatic ketones and industrial pigments (Schemes S1–S3 in Supplementary Materials), and allowed to identify 9,10-anthraquinone (AQ) as the most effective PC, yielding *p*-tolualdehyde (*p*-TALD) as the main oxidation product (Table S1 in Supplementary Materials). With the goal of implementing the process in a sustainable solvent, we found that the reactivity can be exploited in propylene carbonate [23], yielding a similar *p*-TALD production as the one observed in acetonitrile and acetone, Table S1 in Supplementary Materials (it is worth mentioning that in acetone, overoxidation to *p*-toluic acid was previously observed with 2-carboxyanthraquinone, AQ-COOH [20]). Optimization of the reaction conditions (AQ concentration, air or O_2 atmosphere, and light source, Table S2 in Supplementary Materials) enabled a 75% *p*-xylene conversion in 24 h with blue light (405 nm power density 1.5 W cm^{-2}) with *p*-TALD 44% yield and 60% selectivity among oxidation products; it is worth mentioning that the selectivity changes along the progress of the reaction, and reaches higher values of 75% after 6 h, when *p*-TALD yield is 30%). A quantum yield ϕ_{405} of 0.38% associated to *p*-TALD production after 2 h was obtained. The photo-oxidation outcome in propylene carbonate was superior to other solvents investigated, including ionic liquids and dimethylcarbonate (Table S3 in Supplementary Materials).

Importantly, the photooxidation of *p*-xylene was coupled to H_2O_2 formation from dioxygen reduction [13,28,29]. Along photoirradiation, the concentration of H_2O_2 was almost superimposable to the one of *p*-TALD during the first 6 h (Figure 1), where H_2O_2 concentration reached a significant value of 27 mM, not far from state-of-the-art productivity with organic photocatalysts (these were reached under dioxygen atmosphere) [30]. At longer irradiation time, a depletion of H_2O_2 concentration was observed, possibly involving its partial decomposition or its involvement in the oxidation of reaction intermediates.

A similar photochemical reactivity was obtained with 3,6-di-*tert*-butyl-9-mesityl-10-phenyl acridin-10-ium (further abbreviated as Acr^+-1, used as the BF_4^- salt) [31,32], consistent with the activity of this class of PC developed by Fukuzumi and coworkers (see Figure S3 for the absorption spectra of AQ and Acr^+-1) [21]. Optimization of the reaction conditions (2 mM Acr^+-1, air atmosphere, and white or 450 nm blue light) enabled a 80% *p*-xylene conversion in 24 h, with *p*-TALD production with 41% yield and 51% selectivity among oxidation products; simultaneously yielding 11-13 mM H_2O_2 (Figures S4 and S5 and Table S4 in Supplementary Material).

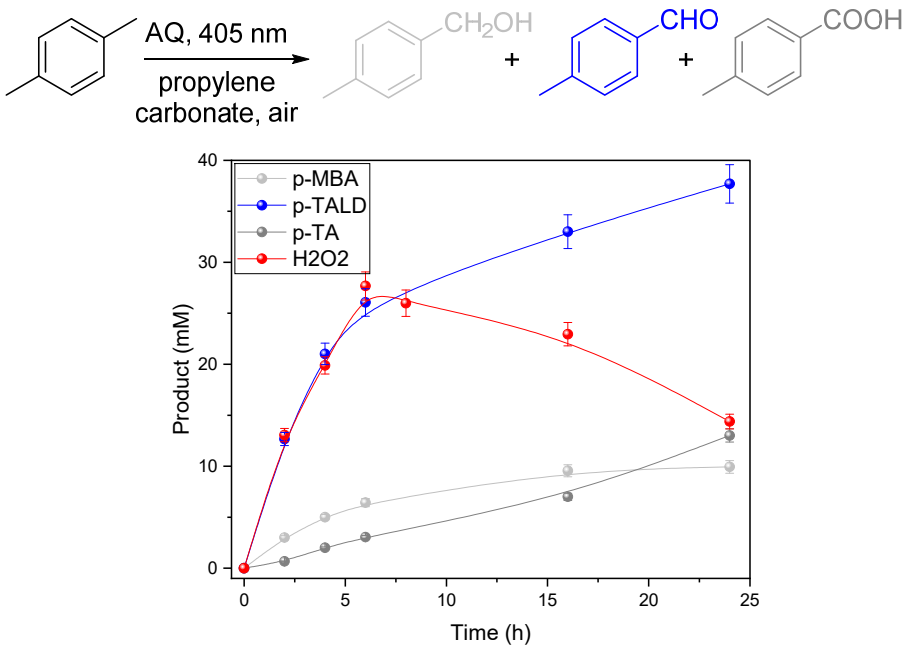

Figure 1. Photocatalytic aerobic oxidation of *p*-xylene (80 mM) in propylene carbonate with AQ (2 mM) under blue light irradiation (LED 405 nm, power density set at 50% corresponding to 1.5 Wcm^{-2}).

The photochemical mechanism was investigated by a combination of laser flash photolysis and EPR. In nitrogen-purged solution, laser excitation at 355 nm of AQ (1 mM in propylene carbonate) leads to the formation of absorption bands at 375, 625, 670 and 800 nm indicative of prompt formation of the triplet excited state ^{3*}AQ (Figure 2A) [33]. These spectral features evolve on a microsecond timescale to a new signal, characterized by an absorption feature at 540 nm, and ascribable to the anthraquinone radical anion, $AQ^{\bullet-}$ [34]. The formation of $AQ^{\bullet-}$ was corroborated by acquiring the EPR signal of $AQ^{\bullet-}$ centered at a *g*-value = 2.004, obtained upon irradiation of an AQ solution in propylene carbonate (Figure 2B) [34]. The simulated spectrum provides hyperfine coupling constants of *a*(4H: 2,3,6,7) = 2.73 MHz and *a*(4H: 1,4,5,8) = 1.02 MHz (Figure 2B), which are in agreement with $AQ^{\bullet-}$ from literature [35]. At longer times of LFP analysis, the progressive abatement of the absorption at 540 nm and the appearance of absorption features in the range 350-450 nm are observed, suggesting a further evolution of $AQ^{\bullet-}$ (see the yellow trace at 1 ms in Figures 2A and S6 showing the kinetic profile of the signature at 540 nm). Consistent diagnostic features are observed upon prolonged irradiation of an AQ solution in degassed propylene carbonate, Figure S7, and are ascribable to bis-reduced derivatives of AQ [36], hereafter indicated AQ^{2-}, formed upon further reduction of $AQ^{\bullet-}$ or by its disproportionation.

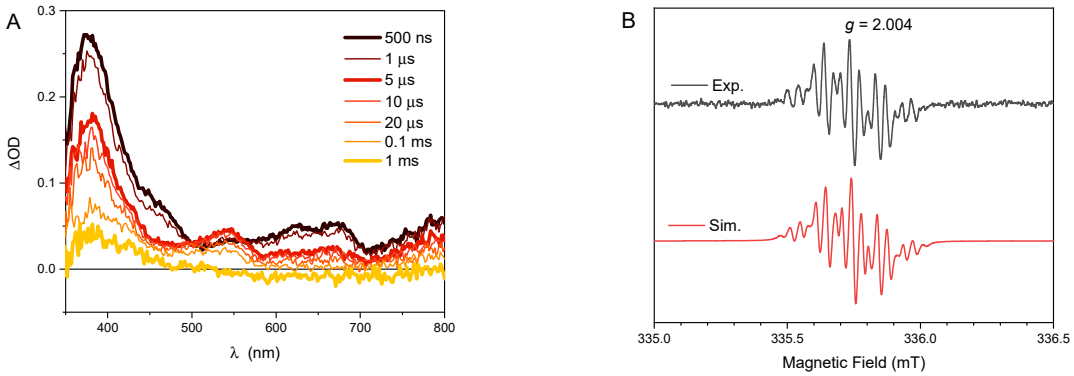

Figure 2. (**A**): LFP of AQ (1 mM in propylene carbonate, degassed) upon laser excitation at 355 nm. Ground state bleaching does not contribute significantly to the spectral features, given the low absorption of the parent anthraquinone in the spectral region examined, see Figure S3. (**B**): experimental and simulated EPR of $AQ^{\bullet-}$, by irradiation (Kessil lamp at 405 nm) of a degassed solution of AQ (2 mM) in propylene carbonate with blue light.

These findings highlight an active role of propylene carbonate solvent in promoting the reductive quenching of AQ, leading to the formation of its reduced species $AQ^{\bullet-}$ and AQ^{2-}. In aerobic atmosphere, these species are expected to be reoxidized to AQ and lead to the formation of reactive oxygen species. Consistently, the formation of superoxide radical anion ($O_2^{\bullet-}$) was confirmed by the observation of the diagnostic EPR signal of DMPO-OOH adduct (Figure S8, DMPO = 5,5-dimethyl-1-pyrroline-*N*-oxide, used as a spin trap) [37], while H_2O_2 formed up to 8 mM upon prolonged irradiation of an aerated 2 mM AQ solution in propylene carbonate (Figure S9, conducted under the same condition of photocatalytic tests, see above discussion). In particular, the accumulation of H_2O_2 reaches lower concentration with respect to the conditions in the presence of *p*-xylene (8 mM in propylene carbonate alone, vs. 27 mM in the presence of 80 mM *p*-xylene, see Figure S9); this prompted us to investigate the mechanism further, in particular focusing on the role of *p*-xylene. LFP experiments conducted in the presence of *p*-xylene (80 mM) did not show significant differences with respect to those obtained for the sole AQ in propylene carbonate previously discussed (see Figure S10). Conversely, one key difference given by the presence of *p*-xylene was the formation of novel EPR features under photoirradiation in the presence of DMPO (Figure 3). In particular, a composite spectrum was observed (black trace in Figure 3), originated from the contributions of DMPO-OOH [37] (diagnostic for the formation of $O_2^{\bullet-}$, red trace in Figure 3, see above discussion) and of a DMPO adduct with carbon based radicals (blue trace in Figure 3) [38]. This evidence is indicative of formation of the benzyl radical from *p*-xylene, obtained via a HAT involving acceptors such as the $^{3*}AQ$ and $O_2^{\bullet-}$. The benzyl radical can partake in chain reactions involving dioxygen, that ultimately lead to *p*-TALD formation. These steps lead to the formation of electrophilic organic peroxide radicals, that feed the chain reaction working as HAT acceptors (Figure 4).

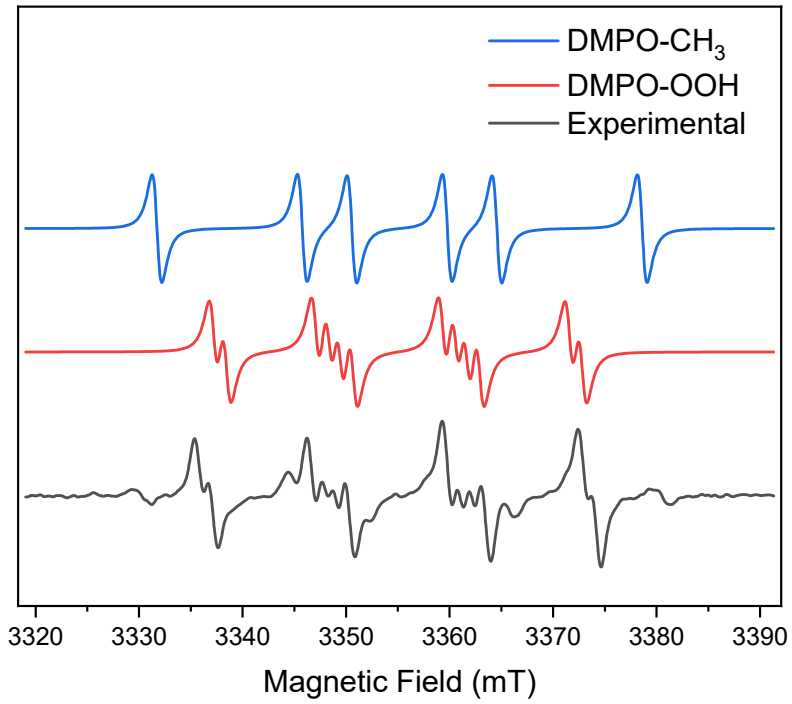

Figure 3. EPR signal obtained upon irradiation of a solution of AQ and *p*-xylene in propylene carbonate (black trace, AQ 2 mM, *p*-xylene 80 mM, aerobic conditions, DMPO 25 mM, 405 nm irradiation), and comparison with simulated signals for DMPO-OOH (red trace) and DMPO-CH_3 (blue trace) adducts, this latter being representative of adducts between DMPO and carbon based radicals. Organic superoxides may contribute to the EPR signal, providing very similar features to the ones of DMPO-OOH adduct (originated from superoxide $O_2^{\bullet-}$ trapping by DMPO, Figure S8).

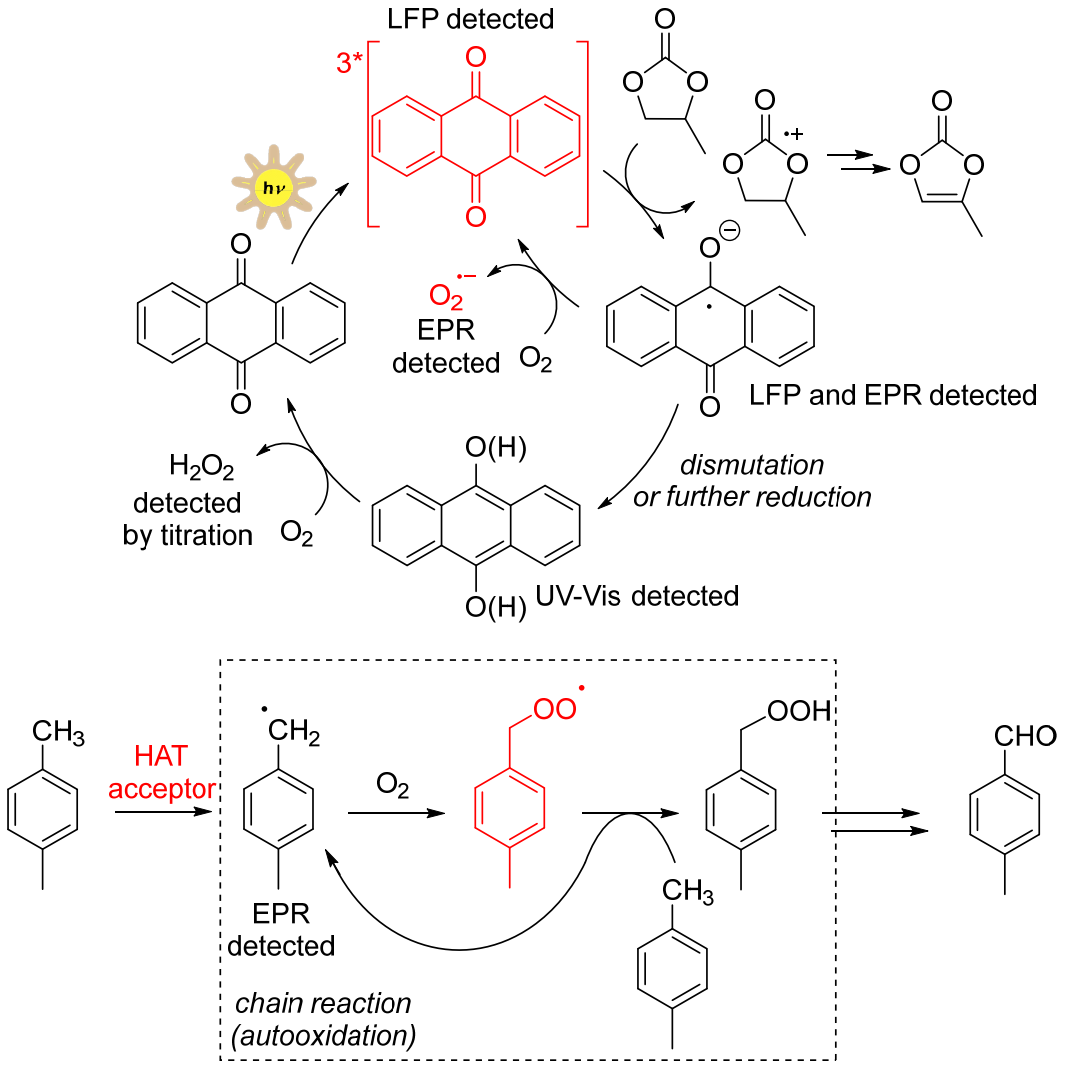

Figure 4. Reaction mechanism, where characterized pertinent intermediates are specified. Species that may be responsible for hydrogen atom abstractions are represented in red.

4. Discussion

The systems developed in this work examined the light driven oxidation of *p*-xylene in aerobic conditions with organic PCs, with AQ and Acr^+-1 being the most active, leading to the main formation of *p*-TALD oxidation product, with similar yield and selectivity. All the experimental findings suggest aerobic chain oxidation driving the oxidation of *p*-xylene to *p*-TALD, concomitant with H_2O_2 production; the overall mechanism is represented in Figure 4 for AQ. The key points are highlighted as follows:

(i) Propylene carbonate solvent retains a non-innocent role, since it is responsible for the reductive quenching of the triplet excited state of anthraquinone ^{3*}AQ leading to the formation of the radical anion $AQ^{\bullet-}$ (detected by LFP and by EPR) and to bis-reduced derivatives of AQ (detected by UV-Vis spectroscopy). A similar outcome was found for Acr^+-1, for which the formation of the acridine radical upon irradiation in propylene carbonate was confirmed by LFP and EPR (Figures S11 and S12) [39,40].

(ii) The reduced forms of AQ are responsible for the formation of superoxide $O_2^{\bullet-}$ (detected by EPR, with spin trap) and hydrogen peroxide (up to 8 mM). The photochemical production of H_2O_2 is indeed an additional benefit for the overall process.

(iii) *p*-xylene is involved in the overall process by reacting with HAT acceptors and generating the benzyl radical (detected by EPR with spin trap), that enters a radical chain process leading to *p*-TALD production and boosting the H_2O_2 production, up to 27 mM concentration.

(iv) Literature systems reporting photocatalytic oxidation of *p*-xylene are reported in Table S4. The most relevant comparisons are with the organic PCs employed in these studies: the anthraquinone derivative AQ-COOH [20] and acridinium Acr^+-Mes [21]. In the case of AQ-COOH, acetone was used as the solvent, and reactive oxygen species were detected and postulated as responsible for the oxidation of *p*-xylene. Detection of hydrogen

peroxide was not mentioned, possibly ascribable to its reactivity with acetone [41], that can be responsible for overoxidation of *p*-TA as observed in this study. Acr^+-Mes was instead investigated in $CH_3CN/H_2O/H_2SO_4$, although a preparative photocatalytic reaction conducted in CH_3CN lead to ca 50% *p*-TALD yield and H_2O_2 production up to ca 16 mM [21]. In this sense, the use of propylene carbonate allows to maintain similar yield and selectivity for *p*-TALD, obtaining H_2O_2 up to 27 mM. A further advantage of propylene carbonate is the possibility of extracting H_2O_2 photoproduced with water, separating it from organic products, exploiting the limited miscibility of this solvent with water. Indeed, we observed a 50% extraction of photoproduced H_2O_2 from the reaction mixture in water by using equivalent volume amounts of the two phases.

(v) Finally, the developed conditions can be extended to other organic substrates carrying benzylic or activated C-H bonds, such as diphenylmethane, ethylbenzene, ethanol, toluene and *o*- and *m*-xylene (Figure 5).

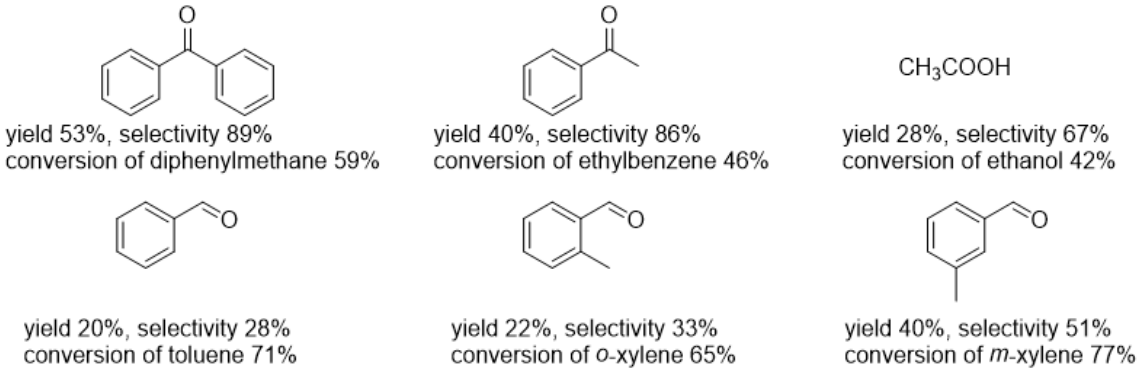

Figure 5. Products obtained from photocatalytic oxidation of substrates with activated C-H bonds (80 mM substrate in propylene carbonate, 2 mM AQ, 405 nm irradiation 1.5 Wcm^{-2}, 24 h).

5. Conclusions

In this work, we demonstrated the aerobic photocatalytic oxidation of *p*-xylene to *p*-tolualdehyde using organic PCs—9,10-anthraquinone and Acr^+-1—in propylene carbonate as a green solvent under visible light irradiation. Optimized conditions achieved up to 80–84% *p*-xylene conversion in 24 h, with *p*- tolualdehyde as the main product (up to 44% yield, 60% selectivity). A key finding of this study is the non-innocent role of propylene carbonate, which actively promotes reductive quenching of $^{3*}AQ$, generating the radical anion $AQ^{\bullet-}$ and bis-reduced species AQ^{2-}, as evidenced by LFP and EPR spectroscopy. Under aerobic conditions, these reduced species drive the formation of ROS—superoxide $O_2^{\bullet-}$ and H_2O_2—the latter reaching concentrations up to 27 mM, representing a valuable co-product of the process. Mechanistic investigation revealed that *p*-xylene oxidation proceeds through a radical chain mechanism initiated by HAT, where benzyl radicals generated from *p*-xylene enter a propagation cycle involving organic peroxide radicals, ultimately yielding the aldehyde. The presence of *p*-xylene also significantly boosts H_2O_2 production compared to solvent-only conditions, highlighting a synergistic effect within the photocatalytic cycle.

Compared to previously reported systems employing AQ-COOH in acetone or Acr^+-Mes in $CH_3CN/H_2O/H_2SO_4$, the use of propylene carbonate as a green solvent maintains comparable or superior performance in terms of *p*-tolualdehyde yield and selectivity, while enabling higher H_2O_2 accumulation and avoiding overoxidation side products. Finally, the photocatalytic conditions proved broadly applicable to other substrates bearing activated C–H bonds, including diphenylmethane, ethylbenzene, ethanol, and xylene isomers, demonstrating the versatility and synthetic potential of this approach.

Overall, this work contributes to the development of sustainable photocatalytic oxidative transformations, combining green solvent selection, visible light activation, and dual valorization through simultaneous fine chemical and H_2O_2 production. Future efforts may focus on further improving selectivity, scaling up the process, and exploring additional substrate scopes under optimized conditions.

Supplementary Materials

The additional data and information can be downloaded at: https://media.sciltp.com/articles/others/260804150506 5058/Photocatalysis-26060133-SM.pdf. References [42,43] are cited in supplementary materials.

Author Contributions

T.W. and A.G.: investigation, writing—original draft preparation; F.D. and L.M.: investigation; L.Đ., M.N. and A.S. conceptualization, methodology, supervision, writing—reviewing and editing. All authors have read and agreed to the published version of the manuscript.

Funding

This research was funded by the University of Padova P-DiSC#06BIRD2025. T.W. acknowledges the Chinese Scholarship Council for a PhD scholarship in the molecular science program, at the department of chemical sciences, university of Padova (Italy). L.Đ. was funded by the European Union (ERC, PhotoDark, 101077698). Views and opinions expressed are however those of the authors only and do not necessarily reflect those of the European Union or the European Research Council. Neither the European Union nor the granting authority can be held responsible for them.

Institutional Review Board Statement

Not applicable.

Informed Consent Statement

Not applicable.

Data Availability Statement

Raw data are available from the authors upon request.

Conflicts of Interest

The authors declare no conflict of interest.

Use of AI and AI-Assisted Technologies

No AI tools were utilized for this paper.

References

1. Xiang, X.; Cheng, B.; Zhu, B.; et al. High-Entropy Alloy Nanocrystals Boosting Photocatalytic Hydrogen Evolution Coupled with Selective Oxidation of Cinnamyl Alcohol. *Chin. J. Catal.* **2025**, *68*, 326–335. https://doi.org/10.1016/S1872-2067(24)60167-1.
2. Bhattacharjee, S.; Linley, S.; Reisner, E. Solar Reforming as an Emerging Technology for Circular Chemical Industries. *Nat. Rev. Chem.* **2024**, *8*, 87–105. https://doi.org/10.1038/s41570-023-00567-x.
3. Barbieri, M.; Cappelletti, D.; Vaccarin, L.; et al. Supramolecular Dye Polymers for Aggregation-Induced Photocatalysis. *Nat. Chem.* **2026**, *18*, 1372–1382. https://doi.org/10.1038/s41557-026-02151-4.
4. Li, X.; Xie, J.; Jiang, C.; et al. Review on Design and Evaluation of Environmental Photocatalysts. *Front. Environ. Sci. Eng.* **2018**, *12*, 14.
5. Wang, H.; Li, X.; Zhao, X.; et al. A Review on Heterogeneous Photocatalysis for Environmental Remediation: From Semiconductors to Modification Strategies. *Chin. J. Catal.* **2022**, *43*, 178–214. https://doi.org/10.1016/S1872-2067(21)63910-4.
6. Ahtasham, M.; Akram, S.; Lal, B.; et al. Advanced Photocatalysis as a Viable and Sustainable Wastewater Treatment Process: A Comprehensive Review. *Environ. Res.* **2024**, *253*, 118947. https://doi.org/10.1016/j.envres.2024.118947.
7. Yang, Y.; Nalesso, M.; Basagni, A.; et al. Photocatalytic Oxidation of Glycerol with Red Light Employing Quinacridone Sensitized TiO_2 Nanoparticles. *J. Mater. Chem. A* **2025**, *13*, 18436–18444. https://doi.org/10.1039/d5ta01970b.
8. Stone, A.E.B.S.; Fortunato, A.; Wang, X.; et al. Photocatalytic Semi-Hydrogenation of Acetylene to Polymer-Grade Ethylene with Molecular and Metal–Organic Framework Cobaloximes. *Adv. Mater.* **2025**, *37*, 2408658. https://doi.org/10.1002/adma.202408658.
9. Uekert, T.; Kuehnel, M.F.; Wakerley, W.; et al. Plastic Waste as a Feedstock for Solar-Driven H_2 Generation. *Energy Environ. Sci.* **2018**, *11*, 2853–2857. https://doi.org/10.1039/c8ee01408f.
10. Oh, S.; Stache, E.E. Chemical Upcycling of Commercial Polystyrene via Catalyst-Controlled Photooxidation. *J. Am. Chem. Soc.* **2022**, *144*, 5745–5749. https://doi.org/10.1021/jacs.2c01411.
11. De Abreu, A.L.; Taton, D.; Bassani, D.M. Reassessing the Photochemical Upcycling of Polystyrene Using Acridinium Salts. *Angew. Chem. Int. Ed.* **2025**, *64*, e202418680. https://doi.org/10.1002/anie.202418680.

12. Skolia, E.; Mountanea, O.G.; Kokotos, C.G. Photochemical Aerobic Upcycling of Polystyrene Plastics. *ChemSusChem* **2024**, *17*, e202400174. https://doi.org/10.1002/cssc.202400174.
13. Tacchi, E.; Rossi, G.; Natali, M.; et al. Aqueous Photocatalytic Glycerol Oxidation to Formic Acid Coupled to H_2O_2 Production with an Anthraquinone Dye. *Adv. Sustain. Syst.* **2025**, *9*, 2400538. https://doi.org/10.1002/adsu.202400538.
14. Tacchi, E.; Anxolabéhère-Mallart, E.; Aukauloo, A.; et al. Catalytic Oxygen Atom Transfer Through Photochemical and Electrochemical Activation of O_2 or H_2O. *Angew. Chem. Novit* **2025**, *1*, e70007. https://doi.org/10.1002/anov.70007.
15. Tacchi, E.; Rossi, G.; Sartorel, A. Photocatalytic Oxidation of Alcohols with Organic Dyes: From Homogeneous Systems to Sensitized Materials. *Chem. Eur. J.* **2025**, *31*, e202501124. https://doi.org/10.1002/chem.202501124.
16. Agarwal, R.G.; Coste, S.C.; Groff, B.D.; et al. Free Energies of Proton-Coupled Electron Transfer Reagents and Their Applications. *Chem. Rev.* **2022**, *122*, 1–49. https://doi.org/10.1021/acs.chemrev.1c00521.
17. Sun, X.; Feng, Z.; Wang, S.; et al. Insight into the Role of TiO_2 Facets in Photocatalytic Selective Oxidation of p-Xylene. *ACS Catal.* **2024**, *14*, 5356–5365. https://doi.org/10.1021/acscatal.4c00543.
18. Lu, Y.; Yu, S.; Jin, J.; et al. Photocatalytic Conversion of *p*-Xylene into *p*-Tolualdehyde with near 100% Selectivity via a Novel Hydroxyl Radical-Mediated Oxygenation Route. *J. Am. Chem. Soc.* **2025**, *147*, 34891–34900. https://doi.org/10.1021/jacs.5c10960.
19. Li, Z.; Dong, Y.; Zeng, Y.; et al. A Continuous-Flow Photocatalytic System for Highly Selective Oxidation of *p*-Xylene to Terephthalic Acid by Decatungstate Catalyst. *Chin. J. Catal.* **2024**, *66*, 282–291. https://doi.org/10.1016/S1872-2067(24)60134-8.
20. Jiang, D.; Zhang, Q.; Yang, L.; et al. Regulating Effects of Anthraquinone Substituents and Additives in Photo-Catalytic Oxygenation of *p*-Xylene by Molecular Oxygen under Visible Light Irradiation. *Renew. Energy* **2021**, *174*, 928–938. https://doi.org/10.1016/j.renene.2021.04.100.
21. Ohkubo, K.; Mizushima, K.; Iwata, R.; et al. Simultaneous Production of *p*-Tolualdehyde and Hydrogen Peroxide in Photocatalytic Oxygenation of *p*-Xylene and Reduction of Oxygen with 9-Mesityl-10-Methylacridinium Ion Derivatives. *Chem. Commun.* **2010**, *46*, 601–603. https://doi.org/10.1039/b920606j.
22. Alberti, M.; Rossi, G.; Boucherabine, D.; et al. Photoactive Fe(III)Pyclen Complexes for Light-Driven Aerobic Oxidation of *p*-Xylene. *Dalton Trans.* **2026**, *55*, 1716–1726. https://doi.org/10.1039/d5dt02534f.
23. Prudlik, A.; Matei, A.; Scherkus, A.; et al. On the Use of Propylene Carbonate and Dimethyl Carbonate as Green Solvents in Organic Electrosynthesis. *Green Chem.* **2025**, *27*, 4280–4288. https://doi.org/10.1039/d4gc06199c.
24. Hou, H.; Zeng, X.; Zhang, X. Production of Hydrogen Peroxide by Photocatalytic Processes. *Angew. Chem. Int. Ed.* **2020**, *59*, 17356–17376. https://doi.org/10.1002/anie.201911609.
25. Josephy, P.D.; Eling, T.; Mason, R.P. The Horseradish Peroxidase-Catalyzed Oxidation of 3,5,3′,5′-Tetramethylbenzidine. Free Radical and Charge-Transfer Complex Intermediates. *J. Biol. Chem.* **1982**, *257*, 3669–3675. https://doi.org/10.1016/s0021-9258(18)34832-4.
26. Đorđević, L.; Jaynes, T.J.; Sai, H.; et al. Mechanical and Light Activation of Materials for Chemical Production. *Adv. Mater.* **2025**, *37*, 2418137. https://doi.org/10.1002/adma.202418137.
27. Stoll, S.; Schweiger, A. EasySpin, a Comprehensive Software Package for Spectral Simulation and Analysis in EPR. *J. Magn. Reson.* **2006**, *178*, 42–55. https://doi.org/10.1016/j.jmr.2005.08.013.
28. Zhang, W.; Gacs, J.; Arends, I.W.C.E.; et al. Selective Photooxidation Reactions Using Water-Soluble Anthraquinone Photocatalysts. *ChemCatChem* **2017**, *9*, 3821–3826. https://doi.org/10.1002/cctc.201700779.
29. Xu, G.; Liang, Y.; Chen, F. Continuously Photocatalytic Production of H_2O_2 with High Concentrations Using 2-Ethylanthraquinone as Photocatalyst. *J. Mol. Catal. A: Chem.* **2016**, *420*, 66–72. https://doi.org/10.1016/j.molcata.2016.04.009.
30. Gryszel, M.; Schlossarek, T.; Wurthner, F.; et al. Water-Soluble Cationic Perylene Diimide Dyes as Stable Photocatalysts for H_2O_2 Evolution. *ChemPhotoChem* **2023**, *7*, e202300070. https://doi.org/10.1002/cptc.202300070.
31. Margrey, K.A.; McManus, J.B.; Bonazzi, S.; et al. Predictive Model for Site-Selective Aryl and Heteroaryl C–H Functionalization via Organic Photoredox Catalysis. *J. Am. Chem. Soc.* **2017**, *139*, 11288–11299. https://doi.org/10.1021/jacs.7b06715.
32. Roth, H.G.; Oliver, S.F.; Campeau, L.; et al. Acridinium-Based Photocatalysts: A Sustainable Option in Photoredox Catalysis. *J. Org. Chem.* **2016**, *81*, 7244–7249. https://doi.org/10.1021/acs.joc.6b01240.
33. Hulme, B.E.; Land, E.J.; Phillips, G.O. Pulse Radiolysis of 9,10-Anthraquinones. *J. Chem. Soc., Faraday Trans. 1* **1972**, *68*, 2003–2012. https://doi.org/10.1039/F19726802003.
34. Hayano, S.; Fujihira, M. The Protonation of Aromatic Hydrocarbon Radical Anions. I. A Comparison of Methods and a Study of the Mechanism. *Bull. Chem. Soc. Jpn.* **1971**, *44*, 1496–1503.
35. Kausche, T.; Sauberlich, J.; Trobitzsch, E.; et al. Photoreduction of 9,10-Anthraquinone by Triethylamine: A Fourier-Transform EPR Study. *Chem. Phys.* **1996**, *208*, 375–390.
36. Gan, H.; Whitten, D.G. A Sterically Controlled Recyclable System: Reversible Photoredox Reactions between Anthraquinone and Hindered Tertiary Amines. *J. Am. Chem. Soc.* **1993**, *115*, 8031–8037.

37. Cle, J.; Siri, D.; Karoui, H.; et al. Assignment of the EPR Spectrum of 5,5-Dimethyl-1-Pyrroline N-Oxide (DMPO) Superoxide Spin Adduct. *J. Org. Chem.* **2005**, *70*, 1198–1203.
38. Villamena, F.A.; Locigno, E.J.; Rockenbauer, A.; et al. Theoretical and Experimental Studies of the Spin Trapping of Inorganic Radicals by 5,5-Dimethyl-1-Pyrroline N-Oxide (DMPO). 1. Carbon Dioxide Radical Anion. *J. Phys. Chem. A* **2006**, *110*, 13253–13258.
39. Horsewill, S.J.; Sharrock, K.M.M.; Fehér, P.P.; et al. Counterintuitive Photochemistry of an Isolated Acridinyl Radical: ConPET via Preassembly, Solvated Electrons or a Long-Lived Excited State? *Angew. Chem. Int. Ed.* **2025**, *64*, e202506701. https://doi.org/10.1002/anie.202506701.
40. MacKenzie, I.A.; Wang, L.; Onuska, N.P.R.; et al. Discovery and Characterization of an Acridine Radical Photoreductant. *Nature* **2020**, *580*, 76–80. https://doi.org/10.1038/s41586-020-2131-1.
41. Oxley, J.C.; Brady, J.; Wilson, S.A.; et al. The Risk of Mixing Dilute Hydrogen Peroxide and Acetone Solutions. *J. Chem. Health Saf.* **2011**, *19*, 27–33. https://doi.org/10.1016/j.jchas.2011.07.010.
42. Attanasio, D.; Suber, L. Aerobic and Anaerobic Photooxidation of *p*-Xylene in the Presence of Phosphotungstic Acid and Its Tetrabutyl Ammonium Salt. *Inorg. Chem.* **1989**, *28*, 3779–3781.
43. Yuan, F.; Cao, P.; Sun, W.; et al. A Green Oxidation Process of *p*-Xylene to Terephthalic Acid through the UV Irradiation-Enhanced Ozonation Process. *Ind. Eng. Chem. Res.* **2024**, *63*, 8208–8215. https://doi.org/10.1021/acs.iecr.4c00895.